Spatiotemporal dynamics of an optical pulse propagating in multimode hollow-core fibers filled with prealigned molecular gases

Lingling Qiao, Ding Wang,* and Yuxin Leng†

State Key Laboratory of High Field Laser Physics, Shanghai Institute of Optics and Fine Mechanics, Chinese Academy of Sciences, Shanghai 201800, China

(Received 29 December 2015; published 22 February 2016)

Spatiotemporal propagation dynamics of optical pulses in a multimode hollow-core fiber filled with prealigned molecular gases is numerically studied. Due to the use of accurate models, several interesting results are obtained, such as the periodic spatiotemporal evolution behavior, the formation of a stable donut-shaped beam profile, and the increasing of pulse energy during frequency upconversion. It is the use of hollow-core fibers that enables these behaviors to be observed. These observations enrich our understanding of optical pulse propagation dynamics and will benefit relevant technologies.

DOI: 10.1103/PhysRevA.93.023832

I. INTRODUCTION

Propagation of ultrashort optical laser pulses in field-free aligned molecular gases has attracted a lot of interest in the past decade for many applications such as controlling and enhancing high-harmonic generation and THz radiation [1,2], elongating plasma tunnel in filamentation [3], nonlinear frequency conversion [4], ultrashort pulse shaping [5–9], emulating and studying systems in other fields of physics [10,11], and so on. Field-free aligned molecular gases can be prepared by nonresonant excitation with an ultrashort laser pulse [12]. Molecular gases with anisotropic polarizability in thermal equilibrium are isotropic to optical laser pulses. However, when interacting with an ultrashort pulse, the molecules will experience a torque which tries to "align" the molecular axis to the polarization of the laser, leading to a rotational wave packet. After the kick of the pulse, the molecular gases will maintain the rotational coherence for a long time. This will manifest as the periodic modulation of refractive index which depends on both the intensity and duration of the exciting pulse. As a result, laser pulses propagating in such prealigned molecular gases will experience the coupling effects in spatial and temporal domains [13,14]. On the other hand, the coherent state and dynamics of the molecular ensemble are also encoded in the pulses affected by such aligned molecules, which can be retrieved to reveal the underlying physics [15,16]. Based on this, we recently proposed a method for measuring rotational parameters of molecular gases by analyzing spectral characteristics of the optical pulse after propagating through a hollow-core fiber (HCF) which is filled with prealigned gas [17]. Confining the gas medium in a waveguide has the advantage of increasing the interaction length. This has already been used in ultrashort pulse shaping and ultrafast spectroscopy. In these studies, the spatial and temporal domains are assumed to be decoupled and only the temporal domain is considered. However, as demonstrated in free-space propagation [13,14], spatiotemporal coupling is inevitable. When the gas medium is confined in hollow-core fibers which are multimode in essence, spatiotemporal coupling occurs in a more profound way. It should be noted that the spatiotemporal nonlinear effects in multimode solid-core fibers have also gained a lot of interest recently for the intriguing propagation dynamics and the potential of increasing power delivery and communication capacity [18,19]. Compared with multimode solid-core fibers, hollow-core fibers filled with prealigned gases offer alternative features due to the time-varying dielectric media.

In this paper, we present a theoretical study of multimode propagation dynamics in HCF filled with prealigned gases. This work is important in two aspects. First, the underlying physics is complex and merits detailed study. Second, the laser technology based on molecular phase modulation will benefit from such insights. Besides the well-known wavelength tuning and spectral broadening, alternative effects are identified, such as the periodic spatiotemporal evolution behavior, the formation of a stable donut-shaped beam profile, and the increasing of pulse energy during frequency upconversion. From these results, previous studies involving prealigned molecular gases confined in HCF should be carefully reconsidered if the spatial domain is neglected.

The rest of the paper is organized as follows. Section II describes the theoretical model used in this work. Due to the potential strong coupling of multimode, weak coupling approximation [20,21] may fail. Therefore, a model that captures the full mode coupling is needed. Section III presents the simulation results with parameters that mimic typical experimental conditions. Section IV gives some discussions on the results. The paper ends with a conclusion in Sec. V.

II. NUMERICAL MODEL

To simulate the spatial-temporal propagation dynamics of optical pulses in HCFs, we use the HCF version of unidirectional pulse propagation equation (UPPE) [22] as follows:

$$\begin{aligned}\partial_z U_m(\omega,z) = &-\frac{\alpha_m}{2}U_m + \mathbf{i}\left(\beta_m - \frac{\omega}{v_g}\right)U_m \\ &+ \frac{\omega}{c^2\beta_m(\omega)2a^2\int_0^1 r\mathbf{d}r\,J_0^2(u_m r)}\vec{e}_s \\ &\times \int_0^a J_0(u_m r/a)\left[\mathbf{i}\omega\frac{\vec{P}(r,\omega)}{\varepsilon_0} - \frac{\vec{j}(r,\omega)}{\varepsilon_0}\right]r\mathbf{d}r,\end{aligned} \tag{1}$$

*wangding@siom.ac.cn
†lengyuxin@siom.ac.cn

where U_m is the fiber mode field in terms of analytical signal; the subscript m indicates the fiber mode order; α_m and β_m are the linear attenuation and dispersion of the fiber mode [23]; v_g is the group velocity of the fundamental mode at the central wavelength of the pulse; $J_0(u_m r/a)$ describes the mode field distribution and is a zero-order Bessel function of the first kind; u_m is the mth zero point of $J_0(x)$; ω, a,c, ε_0 are angular frequency, fiber inner radius, light speed, and permittivity in vacuum, respectively; $P(r,\omega)$ and $j(r,\omega)$ are nonlinear polarization and plasma effects, respectively. The pulse electric field in time domain can be reconstructed according to

$$E(x,y,z,t) = 2\mathrm{Re}\left\{\mathcal{T}_F^{-1}\left[\sum_m U_m(\omega,z)J_0(u_m r/a)\right]\right\}, \quad (2)$$

where $\mathrm{Re}\{\cdots\}$ indicates the real part of a quantity; $\mathcal{T}_F^{-1}$ is the inverse Fourier transform. $|E|^2$ is normalized to the values of optical intensity. For cubic Kerr effect, the nonlinear polarization is $P/\varepsilon_0 = 2n_0 n_2 \mathcal{I} E$ which does not include harmonic generation. $\mathcal{I}$ is the optical pulse intensity envelope. For molecular rotation-induced refractive index change, the polarization can be described as $P(t)/\varepsilon_0 = 4\pi\rho_{\mathrm{nt}}\Delta\alpha^{(0)}[\langle\langle\cos^2\theta\rangle\rangle(t) - 1/3]\mathcal{T}_F^{-1}[f(\omega)E(\omega)]$, where ρ_{nt} is gas density; $\Delta\alpha^{(0)}$ is the polarizability difference between parallel to and perpendicular to the molecular axis, and is taken to be 1.0 $\mathrm{\AA}^3$ at 800 nm; $f(\omega)$ describes the frequency dependence of polarizability difference [7]; $\langle\langle\cos^2\theta\rangle\rangle$ is the ensemble average of molecular gas alignment degree and can be obtained by integration of the time-dependent Schrödinger equation (TDSE) for rotational quantum states [24], or by the perturbative model [25] for computational efficiency,

$$\langle\langle\cos^2\theta\rangle\rangle(t) = \frac{1}{3} + \frac{16\pi\Delta\alpha^{(0)}}{15n_0^2 hc}\sum_{J=0}^{\infty} K_J \mathrm{Im}[S_J(t)], \quad (3)$$

where h is the Planck constant; $S_J(t) = \int_{-\infty}^{t} e^{-\mathbf{i}\omega_J(t-\tau)}\mathcal{I}(\tau)\mathbf{d}\tau$ and ω_J is the Raman angular frequency corresponding to rotation states with quantum numbers J and $J+2$; $K_J = g_J(\rho_{J+2} - \rho_J)(J+1)(J+2)/(2J+3)$ and g_J is the nuclear spin degenerate factor; $\rho_J = \exp[-J(J+1)/k_B T]/\sum_{J=0}^{\infty} g_J(2J+1)\exp[-J(J+1)/k_B T]$ in atomic units. $\mathrm{Im}[\cdots]$ indicates the imaginary part of a quantity. The gas ionization effect is modeled by $j(t)/\varepsilon_0 = cn_0\eta W(\mathcal{I})U_i(\rho_{\mathrm{nt}} - \rho)E/\mathcal{I}$, where $W(\mathcal{I})$ is the ionization rate calculated according to the Perelomov, Popovand, Terent'ev (PPT) model [26]; U_i is the ionization potential; ρ is electron density; $\eta = 1 + (1.5a_2 - 3.75a_4)(\langle\langle\cos^2\theta\rangle\rangle - 1/3) + 4.375a_4(\langle\langle\cos^4\theta\rangle\rangle - 1/5)$ is the molecular rotation-induced modulation factor of the ionization rate and $a_2 = 0.39$, $a_4 = -0.21$ [8]. The plasma effect is modeled by $j(\omega)/\varepsilon_0 = \frac{\tau_c(1+\mathbf{i}\omega\tau_c)}{1+\omega^2\tau_c^2}\frac{e^2}{\varepsilon_0 m_e}\mathcal{T}_F[\rho E]$, where e, m_e, τ_c are electron charge, mass, and collision time, respectively.

Because there are many parameters in the simulations that can be adjusted, only a small subset of the parameter space is explored in this work. The 3-m-long HCF has a diameter of 250 μm and is filled with 500 mbar static nitrogen gas at room temperature. The length of 3 m is the longest HCF used in experiment up to now [27]. We consider only one 0.5-mJ/40-fs full width at half maximum (FWHM) pump pulse at the 800-nm central wavelength. The probe is 0.02 mJ/40 fs/400 nm and has the same polarization as the pump. Both the pump and probe are of the Gaussian-type spatiotemporal profile at the HCF input. The pump and probe pulses are assumed to be coupled optimally into the fiber; i.e., 98% of the pulse energy is coupled to the fundamental mode. In the simulations, the pump pulse is represented by ten modes and the probe pulses 15 modes. It should be noted that both the pump and the probe pulses propagate in their own retarded frames. Due to the different carrier wavelengths of the two pulses, the two retarded frames move at different velocities. The effects induced by such group velocity mismatch are taken into account in the simulations.

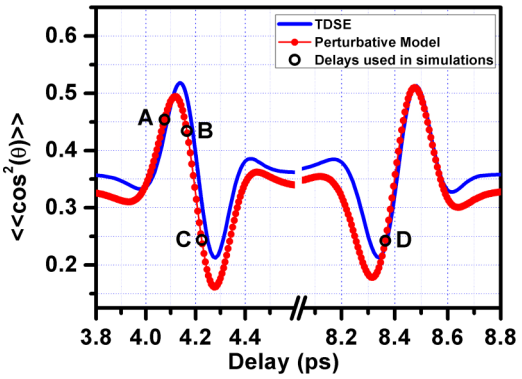

FIG. 1. Molecular alignment obtained with integration of the TDSE (blue solid line) and the perturbative model (red dotted line). The blue solid curve is calculated with both the pump and the probe at a time delay of 4.165 ps. The red dotted curve is obtained with only the pump pulse. The peak of the pump pulse is at time 0. Points A–D are chosen for the later simulations with the corresponding initial time delays (4.075, 4.165, 4.225, and 8.365 ps) for the probe field.

The perturbative model is used to simulate the molecular rotation-induced refractive change. Figure 1 shows the on-axis molecular alignment at the HCF input obtained with TDSE and the perturbative model. The blue solid line indicates the TDSE result which includes the influence of both the pump pulse and the probe at 4.165 ps after the pump. The red dotted line indicates the perturbative result induced by only the pump pulse. It can be seen that although there is difference between the two results, the effects on pulse propagation are almost the same, which means the alignment induced by the probe can be neglected so that the use of the perturbative model is justified. Below, the propagation dynamics of the probe pulse at different delays (A–D in Fig. 1) are studied. The choosing of these delays is based on the following considerations. In the above configurations, the probe pulse propagates slower than the pump. The group delay difference is about 28 fs per meter. Therefore, the delay of the probe after the pump will become larger under linear conditions. For example, at delay A, the probe will first see an increasing of the refractive index with time which leads to redshift in the spectrum, and then a spectral broadening at the highest alignment. After that, the spectrum will undergo blueshift due to the decreasing of refractive index with time. For delay C, the process is reversed. For delay B (D), there is only blueshift (redshift) of the spectrum during the 3 m propagation. These four situations represent the typical

types of propagating evolution in this time-varying medium. When nonlinear effects are taken into account, the dynamics will be more complex.

III. RESULTS

Although this work focuses on the dynamics of the probe pulse, the propagation process of the pump is first described as it determines the following probe. During the 3 m propagation, the pulse energy is localized around the axis of the HCF (see Supplemental Material [28], multimedia 1). The first 0.6 m propagation sees a relatively fast spatiotemporal reshaping due to the mode coupling. After that the spatial profile becomes stable and uniform; the temporal profile changes slowly. After 2 m propagation the temporal profile begins to split. Figure 2(a) shows the normalized total energy of the pump along propagation by the solid dotted line. In the first 0.25 m, the loss rate is high because of the high-order modes and ionization. After 0.6 m, the loss rate becomes constant which is mainly due to the waveguide loss of the fundamental mode. Therefore, the rotation-induced refractive index change for the probe will become smaller along propagation. Figure 2(b) shows the transverse energy distribution of the pump which shows small mode beating. Figure 2(c) shows the temporal distribution of the pump pulse energy along propagation. The walk-off of different modes can also be seen. With such pump, the dynamics of the probe shows a lot of interesting behavior at different delays. The evolution of the 0.02-mJ/400-nm/40-fs pulse without pump in the same HCF is also shown in Figs. 2(a) and 2(d) for comparison in the following.

At delay A (in Fig. 1, at 4.075 ps), the probe is expected to undergo three different spectral shaping processes, i.e., first, redshifting; second, spectral broadening; last, blueshifting. According to the spatiotemporal dynamics of the probe (see Supplemental Material [28], multimedia 2), it is found that the energy of the probe is confined around the axis of the HCF to a smaller radius [also see Fig. 3(b)] than that when the probe propagates without pump [see Fig. 2(d)]. This is easy to understand because the pump created a waveguide in its wake around the delay A where a larger refractive index is induced by a higher alignment degree in the center and a lower refractive

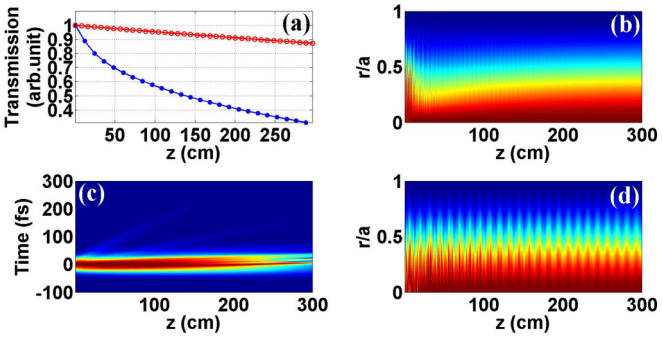

FIG. 2. (a) Normalized pulse energies of a 0.5-mJ/800-nm/40-fs pulse (blue dotted line) and a 0.02-mJ/400-nm/40-fs (red circle line) pulse at different propagation length; transverse energy distributions of the 0.5-mJ/800-nm/40-fs (b) and 0.02-mJ/400-nm/40-fs (d) pulses along propagation; (c) temporal energy distribution of the pump. The distributions are normalized locally.

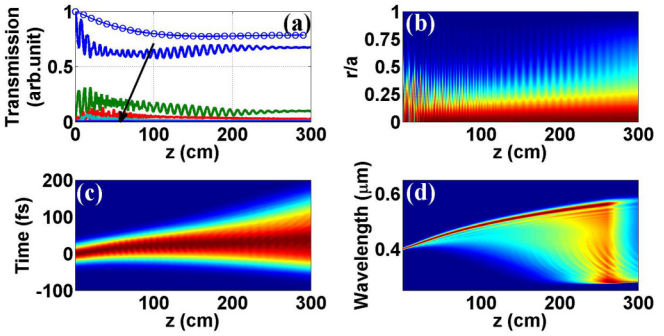

FIG. 3. (a) Energies of different modes (solid lines) and the probe pulse (circles) along propagation length. The values of different modes are normalized at the input energy of the fundamental mode, and the mode order increases along the arrow from 1 to 15; the probe pulse energies are normalized at the input energy; (b) transverse, (c) temporal, and (d) spectral energy distributions of the probe along propagation. The distributions are normalized locally. The delay of the probe is 4.075 ps.

index in the periphery. It should be noted that in the HCF this confinement is extended to several meters, much longer than in free space. With such long confinement, the spectrum is greatly broadened [Fig. 3(d)]. However, there is also pulse splitting in spatiotemporal profiles. The temporal and spectral energy distribution evolutions in Figs. 3(c) and 3(d) are obtained by integrating along the transverse dimension. The pulse splitting appearing in spatiotemporal (spectral) profiles does not show up here. The energies of different modes [shown in Fig. 3(a) by solid lines] show that at least four modes play an important role in the first 0.5 m propagation and then only the first two modes form beating along the propagation. An interesting point is shown in the total probe pulse energy evolution [circles in Fig. 3(a)], i.e., after 1.5 m the probe seems to stop being attenuated and begins to be "amplified" along the propagation although the amplification is negligible. The probe at 1.5 m just passes the highest alignment degree. So this amplification occurs when the probe sees a decreasing refractive index with time. The increase of the pulse energy comes from the rotating molecule ensemble. This represents the other direction of energy exchange between laser pulse and molecule ensemble. The usual direction is the process of excitation of molecular alignment, in which the pulse deposits energy on the molecule ensemble to create a rotational wave packet. The molecular alignment degree can be enhanced or suppressed with more pulses following the first pump pulse, which depends on the delays. If the following pulses kick the molecular ensemble when the alignment degree is increasing, the alignment degree is enhanced; the alignment degree will be suppressed during the decreasing range (see Fig. 1). Because the pulses and the molecular ensemble form a closed system and the highest alignment degree is proportional to the energy deposited on the molecular ensemble, the energy must be extracted from the molecular ensemble and returned to the pulse when the alignment is suppressed. This effect will be more obvious when the initial delay is shifted to B (in Fig. 1, at 4.165 ps).

At delay B, the probe undergoes blueshifting along the propagation. This effect leads to a slower probe [see Fig. 4(c)] as the group delay increases inversely with the central

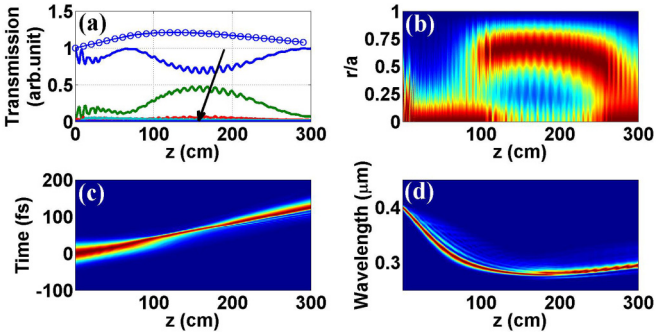

FIG. 4. (a) Energies of different modes (solid lines) and the probe pulse (circles) along propagation length. The values of different modes are normalized at the input energy of the fundamental mode, and the mode order increases along the arrow from 1 to 15; the probe pulse energies are normalized at the input energy; (b) transverse, (c) temporal, and (d) spectral energy distributions of the probe along propagation. The distributions are normalized locally. The delay of the probe is 4.165 ps.

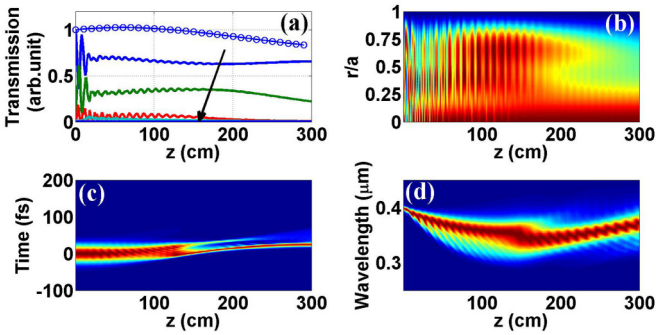

FIG. 5. (a) Energies of different modes (solid lines) and the probe pulse (circles) along propagation length. The values of different modes are normalized at the input energy of the fundamental mode, and the mode order increases along the arrow from 1 to 15; the probe pulse energies are normalized at the input energy; (b) transverse, (c) temporal, and (d) spectral energy distributions of the probe along propagation. The profiles are normalized locally. The delay of the probe is 4.225 ps.

wavelength. However, the blueshift stops when the probe approaches the lowest alignment degree, and then the spectrum begins redshifting. Before redshifting, the probe energy is increasing. As shown in Fig. 4(a), the energy of the probe increases up to more than 10% at 1.1 m, and this is where the blueshifting stops. After this, the simulation results show another interesting behavior; i.e., a stable donut-shaped beam profile is formed between 1.1 and 2.5 m propagation [see Supplemental Material [28], multimedia 3, and Fig. 4(b)]. In this range, the first two modes show a high degree of coupling [Fig. 4(a)], and the spectrum does not change much. But the pulse energy is confined to a much shorter time interval [Fig. 4(c)]. As shown in Fig. 4(b), before 1 m most pulse energy is confined near the HCF axis. Between about 0.6 and 1.1 m, there is a transition for the energy from near the axis to off axis. This is when the probe pulse crosses the zero point of molecular alignment-induced refractive index change, or the transition from focusing to defocusing. In this range, the blueshifting is weak as the pulse energy begins to transfer to the off-axis region where the refractive change is slower. The increasing of pulse energy is also weak due to high-order mode loss. After 2.5 m the pulse energy distribution begins to transfer back to the HCF axis; the spectrum also begins to shift to longer wavelength.

When the probe is delayed 4.225 ps at the input, it immediately sees a defocusing effect. Therefore, the pulse energy distribution tends to expand in the HCF. This can be seen in Fig. 5(b) in which the energy distribution occupies most of the hollow core. The spatiotemporal dynamics (see Supplemental Material [28], multimedia 4) shows another interesting behavior. Before 1.5 m the pulse undergoes rapid spatiotemporal reshaping. After that, a clean and stable pattern emerges which consists of an on-axis component and an off-axis component. The two components are also separated in time by about 20 fs with the off-axis one leading the on-axis one. This pattern lasts up to 2.2 m after which the off-axis component begins to return to the HCF axis. This pattern can also be seen in Fig. 5(c). More energy is in the off-axis component. Both of the two components are confined to a much shorter time interval than the input pulse duration. From Fig. 5(d), it can be seen that there is a transition around a distance of 1.5 m. Before 1.5 m, the spectrum shifts to a shorter wavelength and after that to a longer wavelength, so the pulse arrives at the lowest alignment point near 1.5 m. The pulse energy also stays almost the same before 1.5 m due to the balance of amplification and waveguide loss. Figure 5(a) shows that the second mode keeps a high fraction of total energy over the whole propagation.

At delay D (in Fig. 1, at 8.365 ps), the probe pulse contributes to enhancing molecular alignment along the propagation although this enhancing is negligible. As a result, the energy flows from the pulse to the molecule ensemble. Figure 6(a) shows that the probe energy drops quickly, unlike the above three cases. Because the probe sees an increasing of refractive index, the spectrum will shift to a longer wavelength as shown in Fig. 6(d), and lead to a larger group velocity than the retarded frame at 400 nm. Along the 3 m propagation,

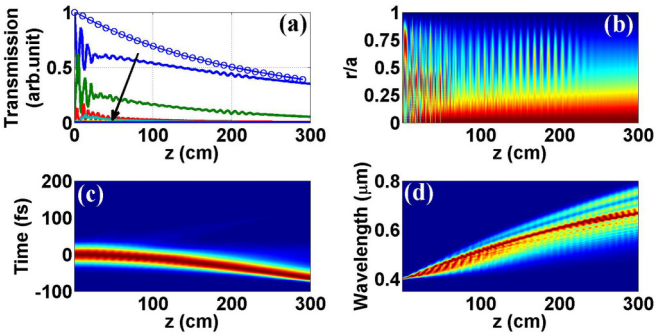

FIG. 6. (a) Energies of different modes (solid lines) and the probe pulse (circles) along propagation length. The values of different modes are normalized at the input energy of the fundamental mode, and the mode order increases along the arrow from 1 to 15; the probe pulse energies are normalized at the input energy; (b) transverse, (c) temporal, and (d) spectral energy distributions of the probe along propagation. The distributions are normalized locally. The delay of the probe is 8.365 ps.

the probe is about 50 fs faster [see Fig. 6(c)]. Considering the retarded frame at 400 nm is 28 fs/m slower than that at 800 nm, the probe pulse will move about 34 fs away from the pump after 3 m propagation. This means the probe will keep seeing a weak defocusing medium in the whole process, and thus the pulse energy will not be localized near the HCF axis as can be seen in Fig. 6(b). Although there is no stable pattern in the spatiotemporal dynamics (see Supplemental Material [28], multimedia 5), a periodic reshaping cycle appears after 1 m and lasts to 2 m. This pattern can also be spotted in Fig. 6(b) in which the transverse energy distribution expands and contracts periodically.

Slightly changing the initial delays of the probe from the above values will lead to similar, although quantitatively different, propagation dynamics. It should be noted that although the current study only involves a specific configuration and a small subset of the whole parameter space, the above cases represent typical spatiotemporal dynamics of pulses in a confined time-varying dielectric medium.

IV. DISCUSSIONS

The advantage of using an HCF for confining the medium and guiding wave propagation is the extension of interaction length. Compared with free-space propagation, a much longer prealigned molecular gas can be prepared. Therefore, in the focusing regime of the wake (e.g., delays A, B) the probe can be guided until either it falls out of this regime due to the different velocities from the pump or the pump is too weak to induce enough alignment degree. As a result, a large wavelength tuning range can be achieved, which has already been reported. A more interesting result is the possibility of achieving a significant increasing of pulse energy at proper delays. This requires long, intense interaction length. We point out here that in this process the number of photons is conserved [29], so that the increase of single-photon energy leads to energy increasing. From the mathematical point of view, it is the transformation of $i\omega^2/\beta_1(\omega)$ in the frequency domain to $-\frac{\partial}{\partial t}$ in the time domain in Eq. (1) that induces an energy change due to rotation-induced refractive index during propagation. Therefore, the nonlinear Schrödinger equation (NLSE) which uses narrow-band approximation will not capture this effect.

When the probe propagates in the defocusing regime, complex spatiotemporal dynamics emerges because of the confinement of the HCF. This will not be observed in free-space propagation. In the defocusing regime (near the lowest antialignment point in Fig. 1), the refractive index of the gas in the HCF is the lowest in the center and gradually increases towards the fiber clad. It is interesting to note that two different initial delays result in stable propagation patterns in this defocusing regime (see Supplemental Material [28], multimedia 2 and 3). Although these propagation patterns can be represented by superposition of the first several eigenmodes of the HCF which have very different dispersion curves, the pulse energy is confined to a very short time interval for a long distance until either the probe falls out of a specific delay range or the pump is too weak to induce enough alignment. The temporal behavior here looks like that of a soliton. We did further more accurate simulations by replacing the perturbative calculation of molecular alignment with integration of TDSE and obtained similar results.

In this work, the nonlinear effects induced by the probe itself are relatively weak. When the probe energy is increased, the spatiotemporal dynamics will be more complex. Furthermore, the choice of the pump and probe parameters and the diameter of the HCF will also have a big influence. These topics need to be studied in the future.

V. CONCLUSIONS

We perform a numerical study of optical pulse propagation in a multimode hollow-core fiber filled with prealigned molecular gases. Due to the use of accurate models, several interesting results are obtained, such as the periodic spatiotemporal shaping behavior, the formation of a stable donut-shaped beam profile, and the increasing of pulse energy during frequency upconversion. According to these results, previous studies involving prealigned molecular gases confined in HCFs should be carefully reconsidered if the spatial domain is neglected. From our simulations, it can be seen that when the probe propagates in the delay range of the focusing regime, the approximation of neglecting the spatial domain may be valid. However, in the defocusing regime, spatiotemporal coupling must be considered. These observations enrich our understanding of the propagation dynamics in HCFs, and will benefit relevant technologies based on similar configurations.

ACKNOWLEDGMENT

This work is supported by National Natural Science Foundation of China (NSFC) (Grant No. 11204328).

[1] R. Velotta, N. Hay, M. B. Mason, M. Castillejo, and J. P. Marangos, Phys. Rev. Lett. **87**, 183901 (2001).
[2] J. Wu, Y. Tong, M. Li, H. Pan, and H. Zeng, Phys. Rev. A **82**, 053416 (2010).
[3] H. Cai, J. Wu, H. Li, X. Bai, and H. Zeng, Opt. Express **17**, 21060 (2009).
[4] B. A. Bartels, N. L. Wagner, M. D. Baertschy, J. Wyss, M. M. Murnane, and H. C. Kapteyn, Opt. Lett. **28**, 346 (2003).
[5] N. Zhavoronkov and G. Korn, Phys. Rev. Lett. **88**, 203901 (2002).
[6] R. A. Bartels, T. C. Weinacht, N. Wagner, M. Baertschy, C. H. Greene, M. M. Murnane, and H. C. Kapteyn, Phys. Rev. Lett. **88**, 013903 (2001).
[7] V. Kalosha, M. Spanner, J. Herrmann, and M. Ivanov, Phys. Rev. Lett. **88**, 103901 (2002).
[8] J. Wu, H. Cai, A. Couairon, and H. Zeng, Phys. Rev. A **79**, 063812 (2009).
[9] F. Wang, H. Jiang, and Q. Gong, J. Opt. Soc. Am. B **29**, 232 (2012).
[10] J. Floss and I. S. Averbukh, Phys. Rev. Lett. **113**, 043002 (2014).

[11] M. F. Saleh, A. Armaroli, T. X. Tran, A. Marini, F. Belli, A. Abdolvand, and F. Biancalana, Opt. Express **23**, 11879 (2015).
[12] B. Friedrich and D. Herschbach, Phys. Rev. Lett. **74**, 4623 (1995).
[13] F. Calegari, C. Vozzi, S. Gasilov, E. Benedetti, G. Sansone, M. Nisoli, S. De Silvestri, and S. Stagira, Phys. Rev. Lett. **100**, 123006 (2008).
[14] F. Calegari, C. Vozzi, and S. Stagira, Phys. Rev. A **79**, 023827 (2009).
[15] J. Itatani, J. Levesque, D. Zeidler, H. Niikura, H. Pepin, J. C. Kieffer, P. B. Corkum, and D. M. Villeneuve, Nature **432**, 867 (2004).
[16] T. Kanai, S. Minemoto, and H. Sakai, Nature **435**, 470 (2005).
[17] D. Wang, L. Qiao, Z. Huang, and Y. Leng, J. Opt. Soc. Am. B **32**, 2238 (2015).
[18] L. G. Wright, D. N. Christodoulides, and F. W. Wise, Nat. Photonics **9**, 306 (2015).
[19] L. G. Wright, S. Wabnitz, D. N. Christodoulides, and F. W. Wise, Phys. Rev. Lett. **115**, 223902 (2015).
[20] G. Tempea and T. Brabec, Opt. Lett. **23**, 1286 (1998).
[21] C. Courtois, A. Couairon, B. Cros, J. R. Marques, and G. Matthieussent, Phys. Plasma **8**, 3445 (2001).
[22] M. Kolesik, and J. V. Moloney, Phys. Rev. E **70**, 036604 (2004).
[23] E. A. Marcatili and R. A. Schmeltzer, Bell Syst. Tech. J. **43**, 1783 (1964).
[24] J. Ortigoso, M. Rodriguez, M. Gupta, and B. Friedrich, J. Chem. Phys. **110**, 3870 (1999).
[25] N. Berti, P. Bejot, J.-P. Wolf, and O. Faucher, Phys. Rev. A **90**, 053851 (2014).
[26] L. Berge, S. Skupin, R. Nuter, J. Kasparian, and J.-P. Wolf, Rep. Prog. Phys. **70**, 1633 (2007).
[27] V. Cardin, N. Thire, S. Beaulieu, V. Wanie, F. Legare, and B. E. Schmidt, Appl. Phys. Lett. **107**, 181101 (2015).
[28] See Supplemental Material at http://link.aps.org/supplemental/10.1103/PhysRevA.93.023832 for movies of spatiotemporal dynamics of the pump pulse (multimedia 1) and the probe pulse at different delays (multimedia 2∼5).
[29] B. W. Plansinis, W. R. Donaldson, and G. P. Agrawal, Phys. Rev. Lett. **115**, 183901 (2015).